Supplementary Information (SI) for Journal of Materials Chemistry B.

Supporting information

Light-mediated activation of nitric oxide and antibacterial polymers for anti-biofilm applications

Siyuan Luo,[a] Zuotao Zhou,[a] Yu Jin,[a] Haochuan Ding,[a] Faxing Jiang,*[c] and Zhiqiang Shen*[a,b]

[a] School of Biomedical Engineering, Division of Life Sciences and Medicine, University of Science and Technology of China, Hefei, Anhui Province, 230026, China. E-mail: shenzq@ustc.edu.cn

[b] Suzhou Institute for Advanced Research, University of Science and Technology of China, Suzhou, 215123, China.

[c] Department of Dermatology, the First Affiliated Hospital-University of Science and Technology of China (Anhui Provincial Hospital), Hefei, Anhui Province, 230001, China. E-mail: jiangfxing@ustc.edu.cn

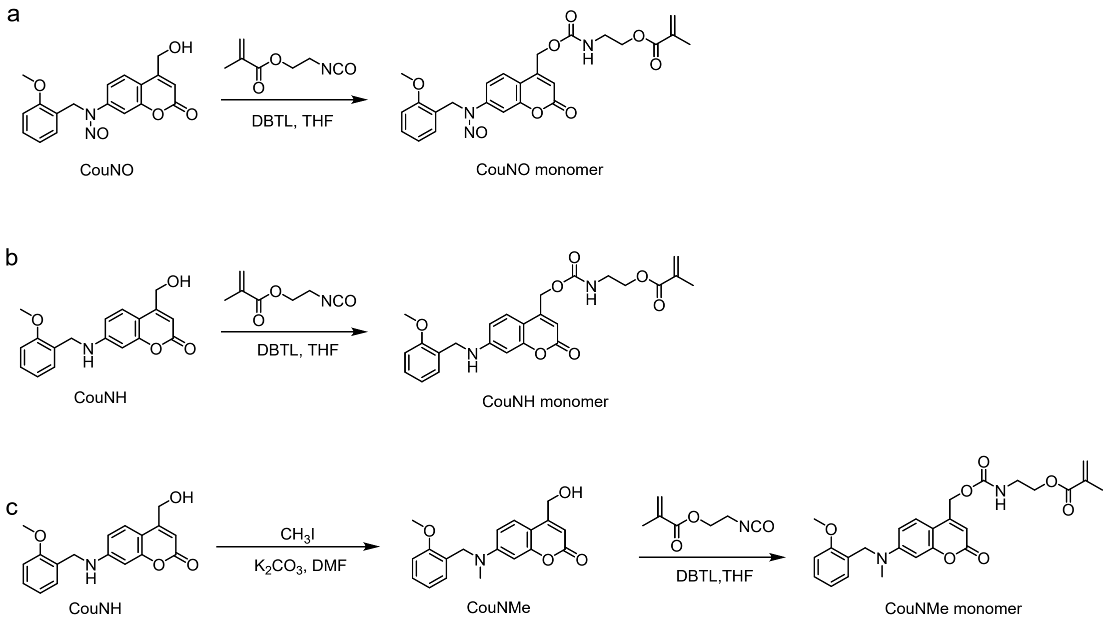

Scheme S1 Synthetic routes of (a) CouNO monomer, (b) CouNH monomer, and (c) CouNMe monomer.

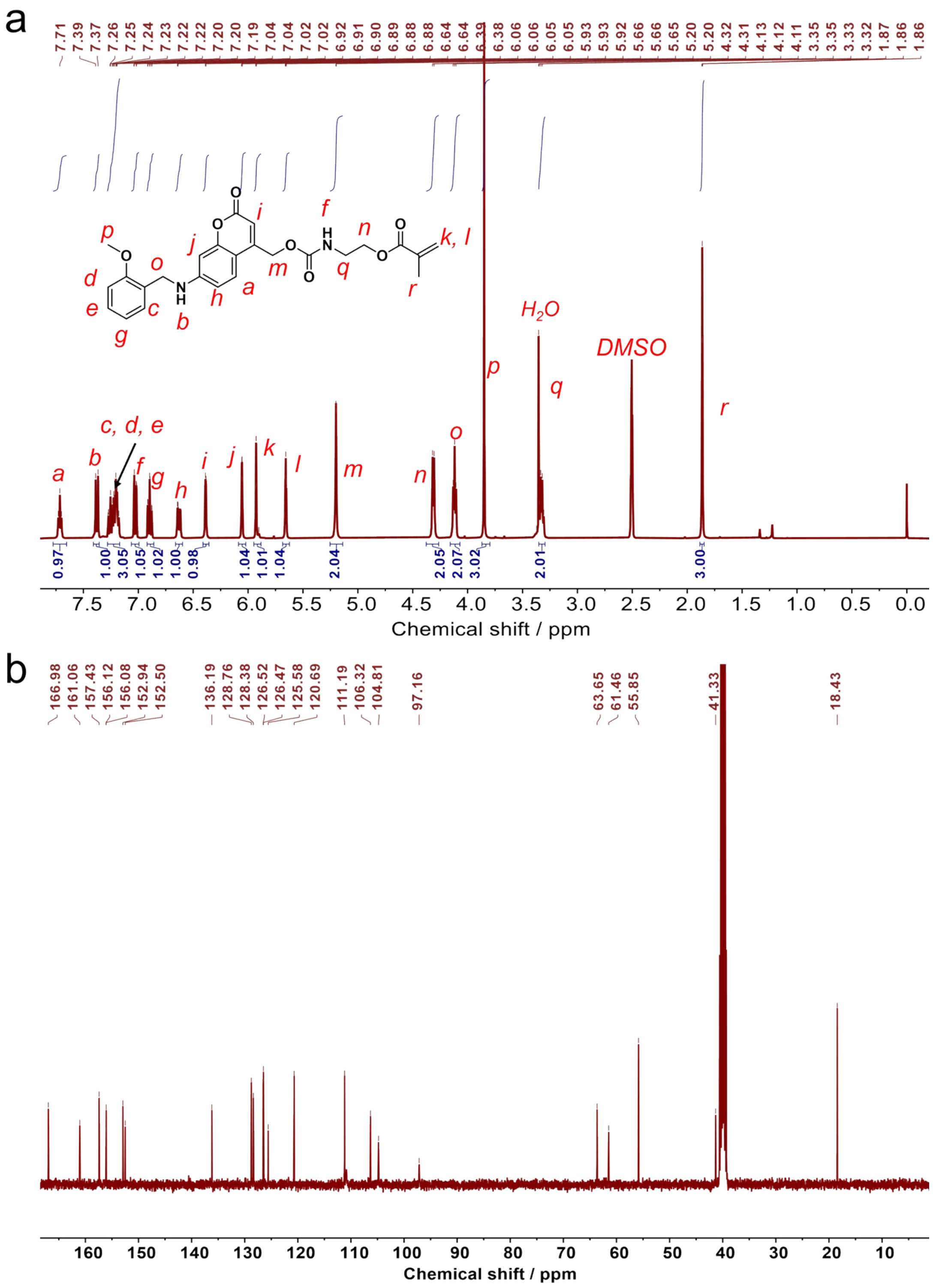

Fig. S1 (a) ^{1}H NMR and (b) ^{13}C NMR spectra recorded in DMSO-d_6 for CouNH monomer.

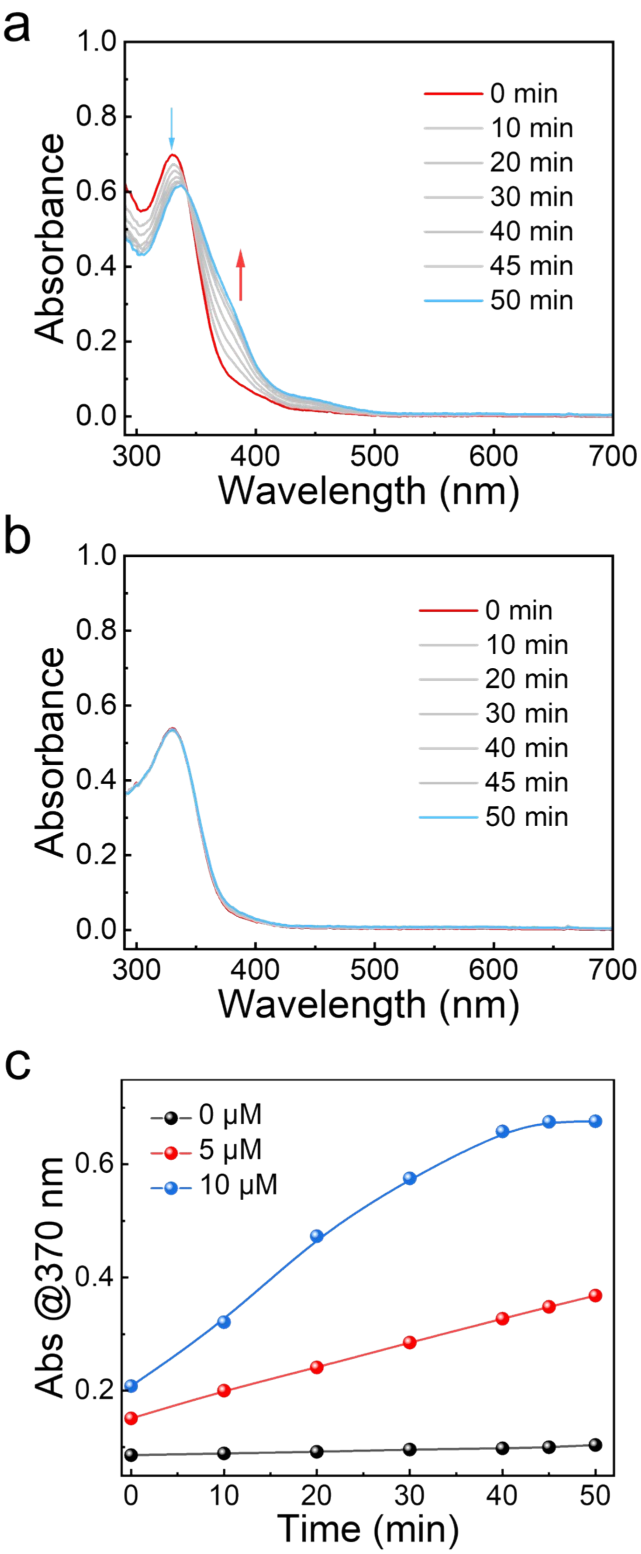

Fig. S2 Evolution of UV-vis spectra of CouNO monomer (50 μM) in the presence of (a) 0, (b) 5 μM *fac*-Ir(ppy)$_3$ in DMSO under 500 nm light irradiation (30 mW/cm^2). (c) Time-dependent changes of absorption intensities at 370 nm of CouNO monomer (50 μM) under above conditions and the presence of 10 μM *fac*-Ir(ppy)$_3$ in DMSO under 500 nm light irradiation (30 mW/cm^2).

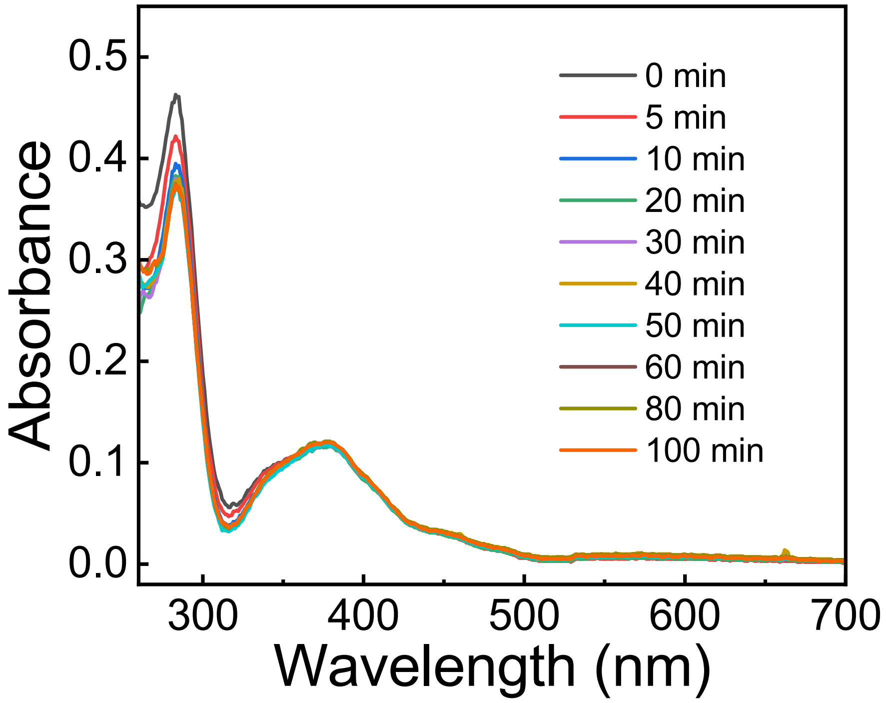

Fig. S3 Evolution of UV-vis spectra of 10 μM *fac*-Ir(ppy)$_3$ in DMSO under 500 nm irradiation (30 mW/cm^2).

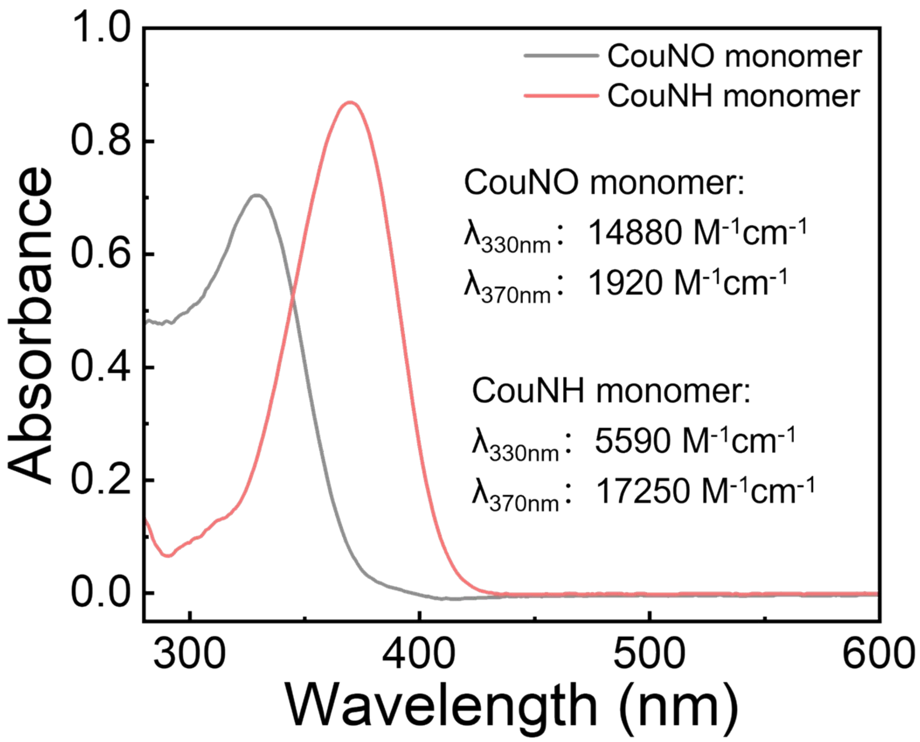

Fig. S4 UV-vis absorbance spectra in DMSO and corresponding extinction coefficients of CouNO monomer and CouNH monomer.

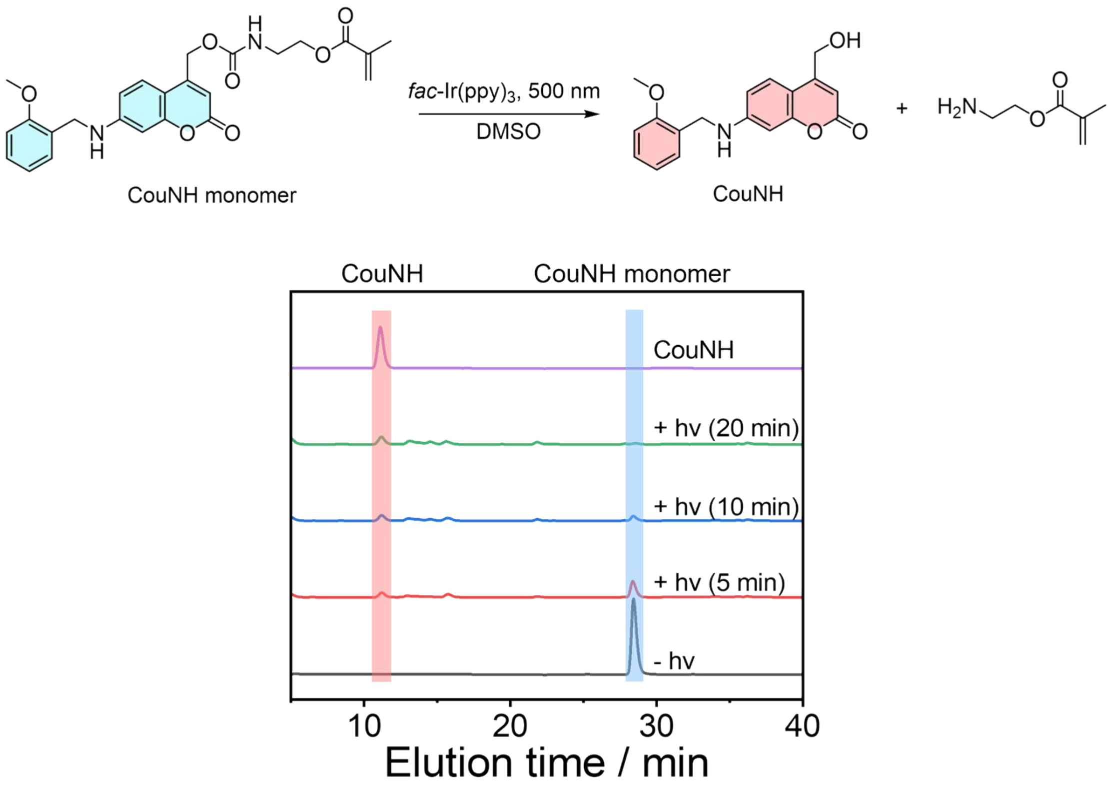

Fig. S5 HPLC trace recorded for sequential degradation of compound CouNH monomer under the light irradiation (500 nm, 30 mW/cm^2) with *fac*-Ir(ppy)$_3$.

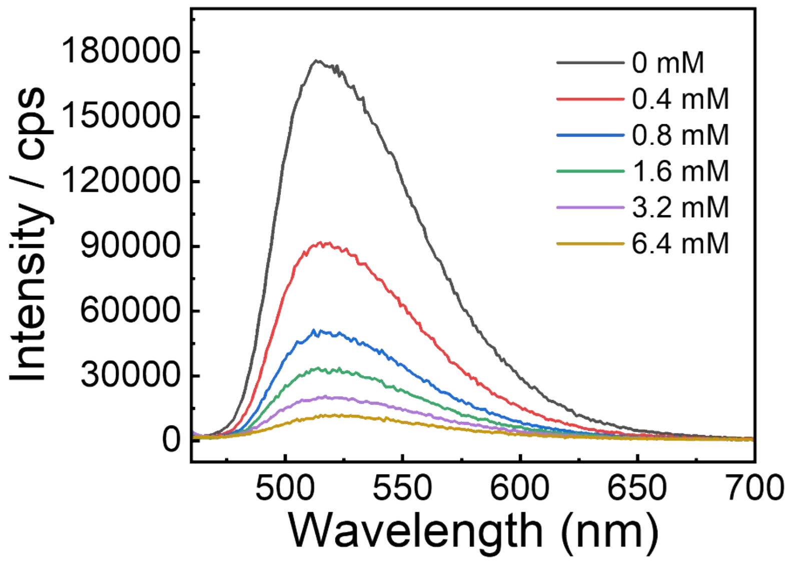

Fig. S6 Steady-state emission spectra (λ_{ex} = 455 nm) of *fac*-Ir(ppy)$_3$ (10 μM) in the presence of varying concentrations of CouNO monomer in deoxygenated DMF.

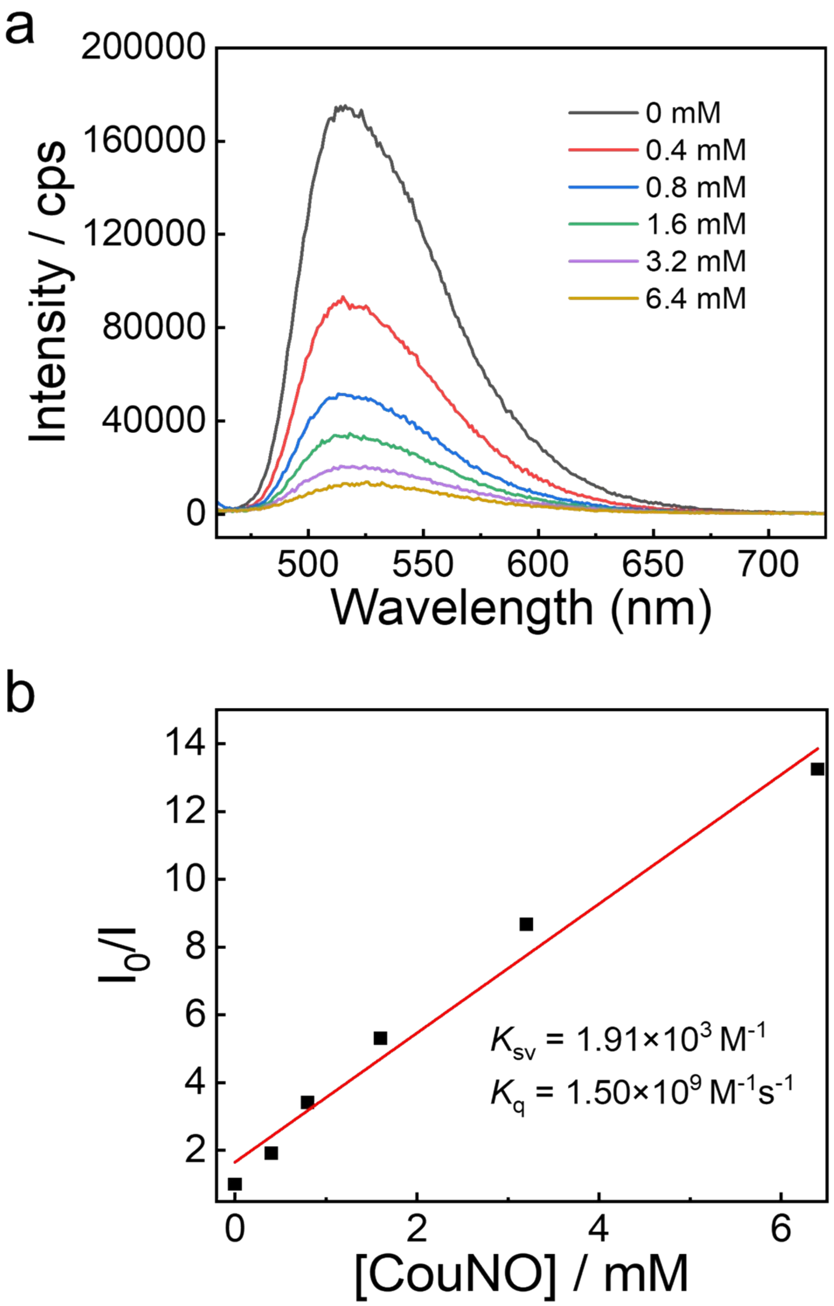

Fig. S7 (a) Steady-state phosphorescence intensity changes (λ_{ex} = 455 nm) of *fac*-Ir(ppy)$_3$ (10 μM) in the presence of varying concentrations of CouNO in Ar-saturated DMF. (b) Stern-Volmer plot of phosphorescence intensity quenching of *fac*-Ir(ppy)$_3$ (10 μM) by CouNO in Ar-saturated DMF.

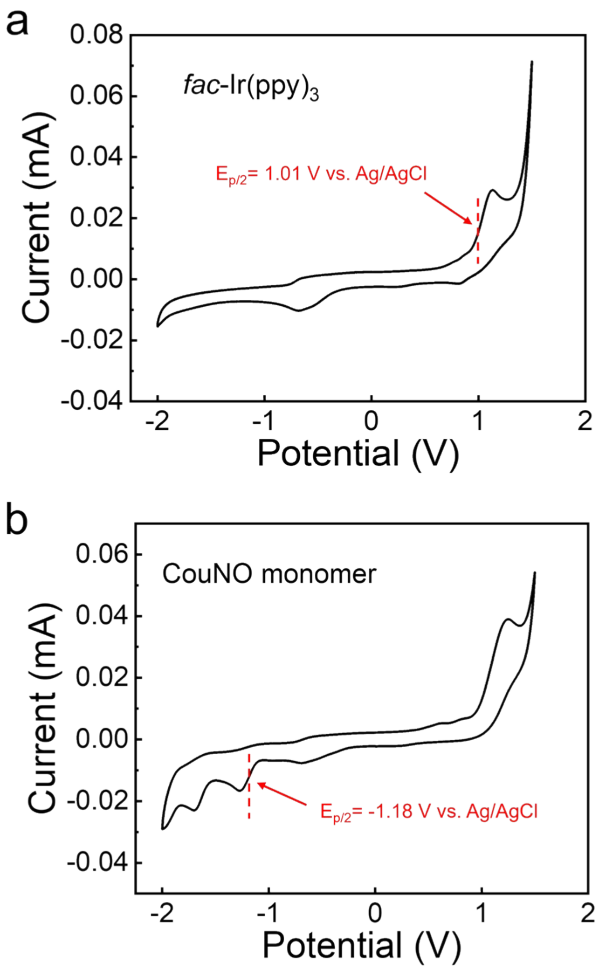

Fig. S8 Cyclic voltammogram curves of (a) *fac*-Ir(ppy)$_3$, (b) CouNO monomer, in DMF (0.1 M Bu_4NBF_4) (scan rate, 0.1 V/s). In all measurements, the concentration of all samples was 1 mM.

Note. Cyclic voltammetry was conducted using 0.1 M tetrabutylammonium tetrafluoroborate as the electrolyte in DMF at 25 °C with an Ag/AgCl reference electrode. The maximal luminescence wavelength of *fac*-Ir(ppy)$_3$ was estimated to be 517 nm (Fig. S6), and the $E_{1/2}^{ox}$ of *fac*-Ir(ppy)$_3$ was determined to be + 1.01 V (vs Ag/AgCl). Using the maximal luminescence wavelength and $E_{1/2}^{ox}$, the excited state reduction potential of *fac*-Ir(ppy)$_3$ was estimated according to the following equations:

$$E_{1/2}([\mathit{fac}\text{-Ir(ppy)}_3]^+/[\mathit{fac}\text{-Ir(ppy)}_3]^*) = E_{1/2}^{ox} - E_{0,0}$$

$$E_{0,0} = hc/\lambda_{max} = 1240\ \text{nm}/\lambda_{max}$$

As such, the excited state reduction potential was calculated to be $E_{1/2}([\mathit{fac}\text{-Ir(ppy)}_3]^+/[\mathit{fac}\text{-Ir(ppy)}_3]^*) = E_{1/2}^{ox} - E_{0,0} = 1.01\ \text{V} - 1240\ \text{nm}/517\ \text{nm} = -1.39\ \text{V}$.

Table. S1 Properties of NO donor and photosensitizer used in this study.

Entry	S_1 (eV)[a]	T_1 (eV)[b]	LUMO (eV)[c]	HOMO (eV)[d]
fac-Ir(ppy)$_3$	2.96	2.40	-1.70	-5.41
CouNO monomer	3.09	2.24	-2.47	-6.37
CouNH monomer	3.41	2.46	-1.95	-5.64
CouNO	3.09	2.23	-2.44	-6.36

[a] Singlet energy (eV). [b] Triplet energy (eV). [c] Lowest unoccupied molecular orbital (eV). [d] Highest occupied molecular orbital (eV).

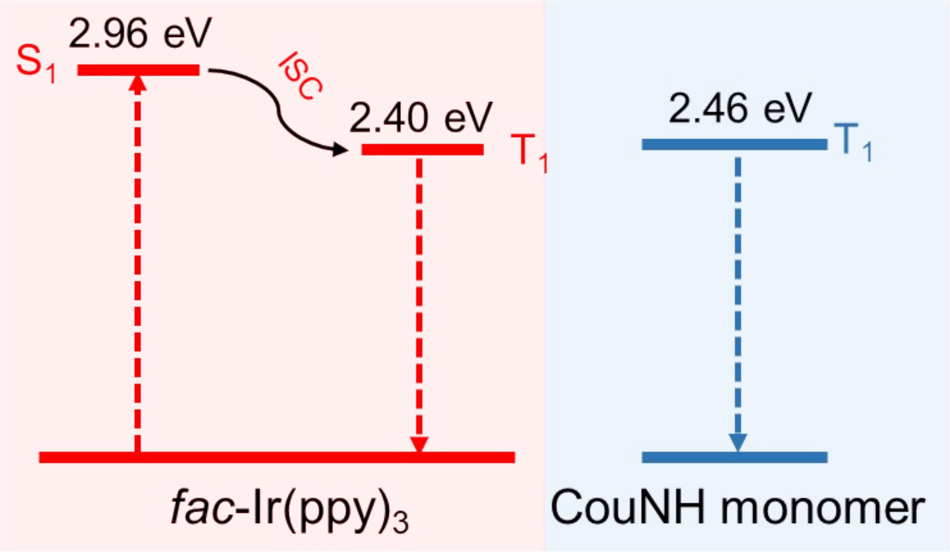

Fig. S9 The singlet (S_1) and triplet (T_1) energy levels of *fac*-Ir(ppy)$_3$ and T_1 energy levels of CouNH monomer.

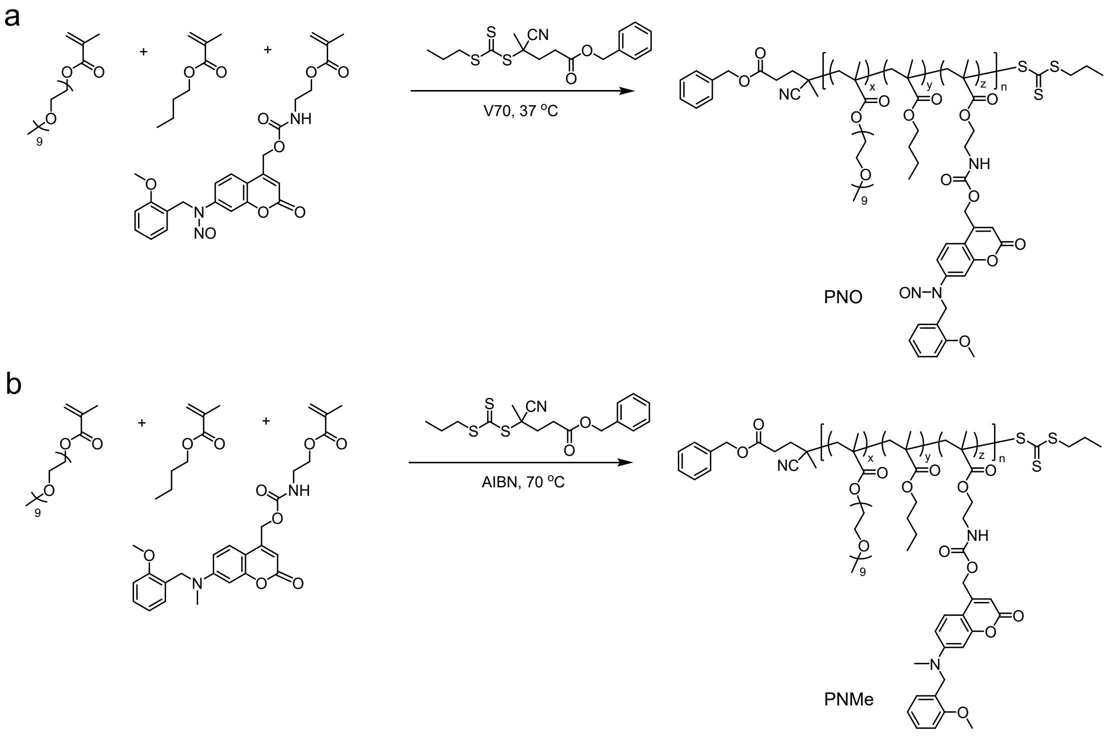

Scheme S2 Synthetic routes of (a) PNO and (b) PNMe.

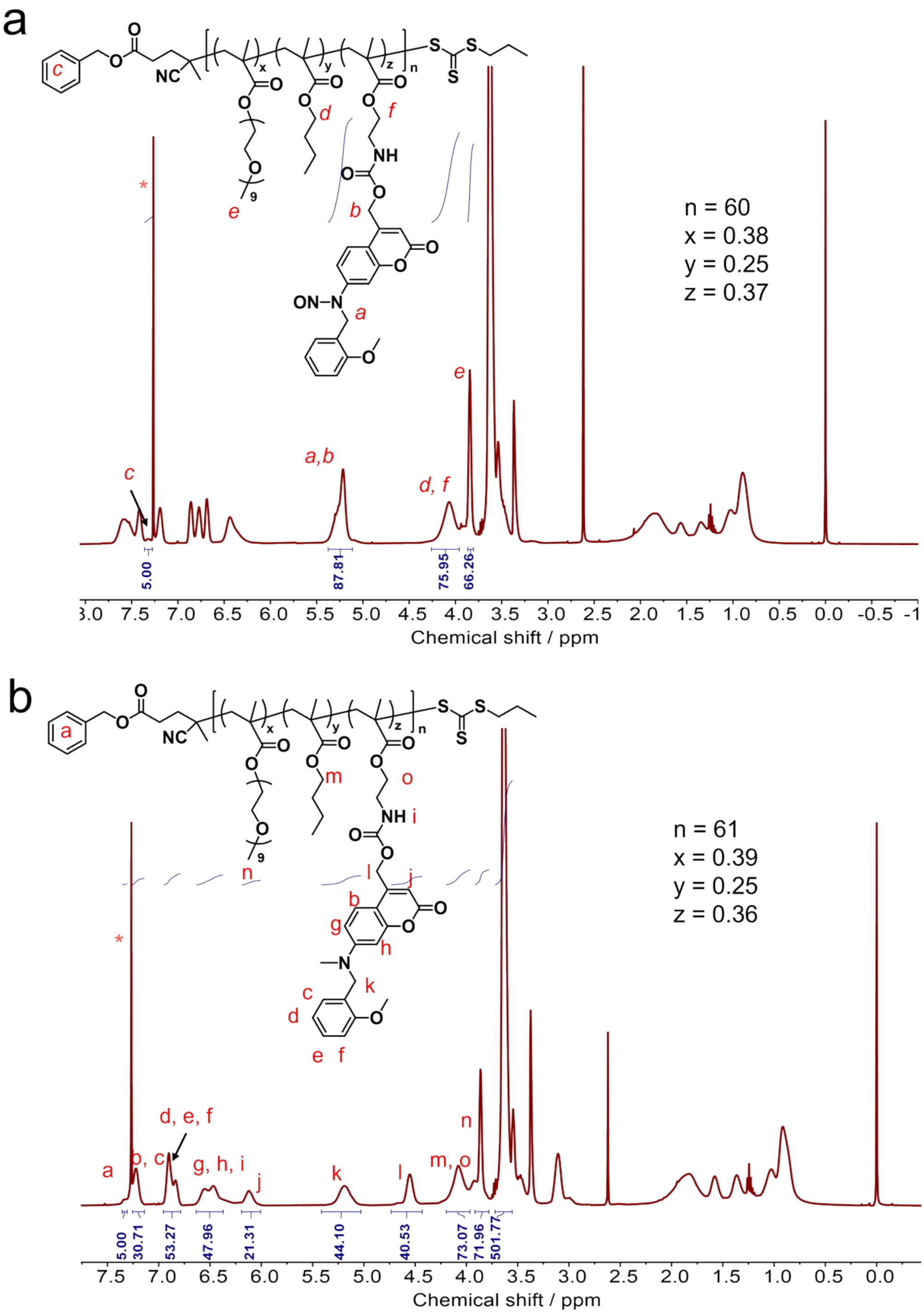

Fig. S10 ^{1}H NMR spectra recorded in $CDCl_3$ for (a) PNO and (b) PNMe.

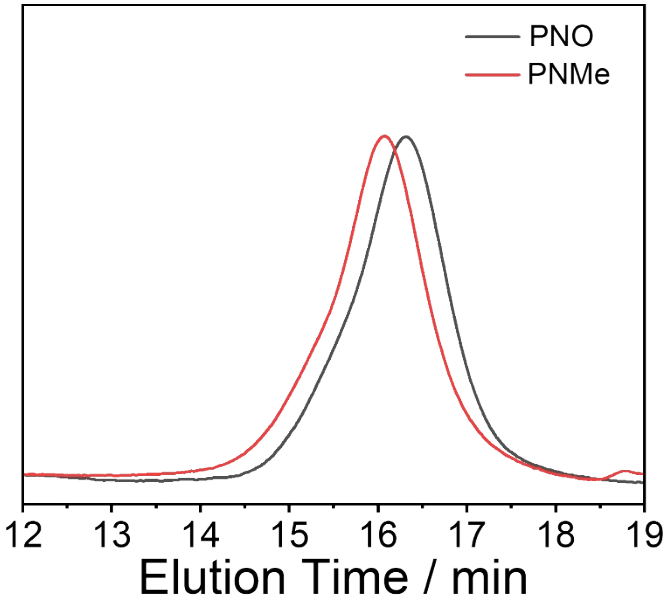

Fig. S11 GPC elution profiles of PNO and PNMe.

Table. S2 Structural parameters of the amphiphilic copolymers used in this study.

Entry	**Chemical composition**[a]	$M_{n,\ NMR}$ [a] **(kDa)**	$M_{n,\ SEC}$ [b] **(kDa)**	M_w/M_n [b]
PNO	P(OEGMA$_{0.38}$-*co*-BMA$_{0.25}$-*co*-CouNO$_{0.37}$)$_{60}$	24.5	21.5	1.25
PNMe	P(OEGMA$_{0.39}$-*co*-BMA$_{0.25}$-*co*-CouNMe$_{0.36}$)$_{61}$	25.0	25.8	1.27

[a] calculated from ^{1}H NMR results; [b] determined by GPC using THF as the eluent.

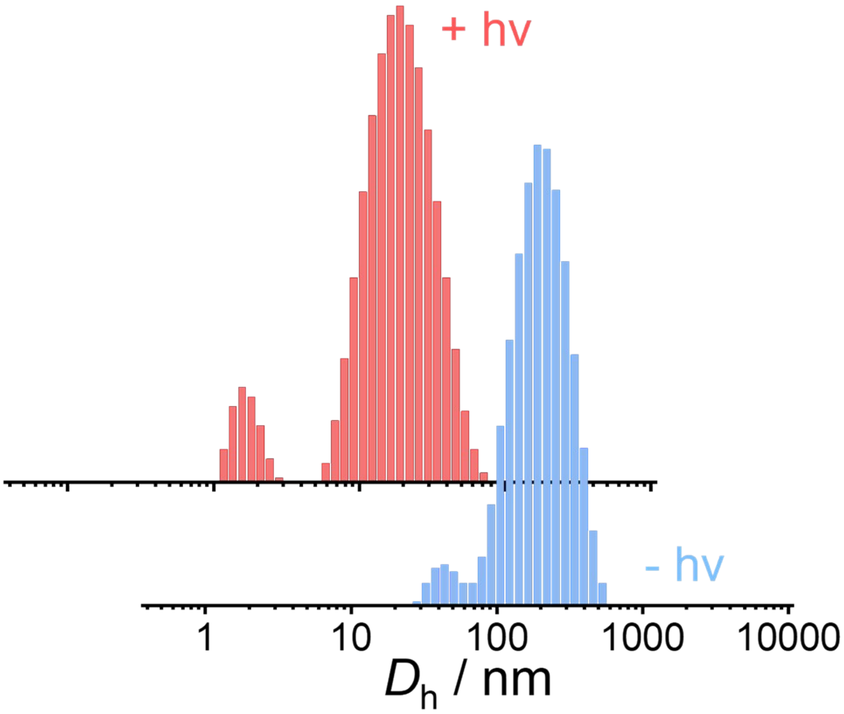

Fig. S12 Intensity-average hydrodynamic diameter distributions of PNO@Ir micelles with or without 500 nm irradiation for 30 min at pH 7.4, respectively. In all cases, the irradiation intensity was 30 mW/cm^2 under a hypoxic condition.

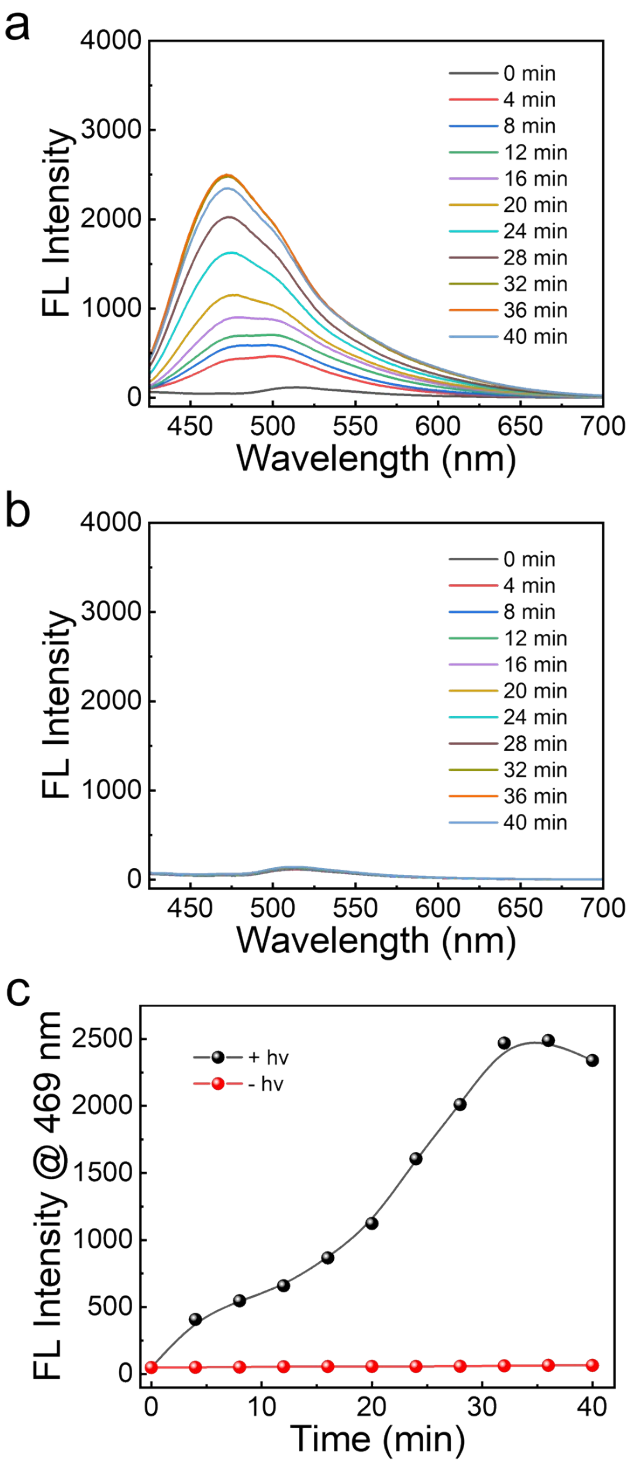

Fig. S13 Fluorescence emission spectra (λ_{ex} = 405 nm) of aqueous dispersions (0.2 g/L) of PNO@Ir in the presence of sodium ascorbate (10 mM) (a) with and (b) without 500 nm light irradiation. (c) Fluorescence intensity changes (λ_{ex} = 405 nm, slit width: E_x. 10 nm; E_m. 10 nm) of solution (0.2 g/L) of PNO@Ir in the presence of sodium ascorbate (10 mM) with and without 500 nm light irradiation.

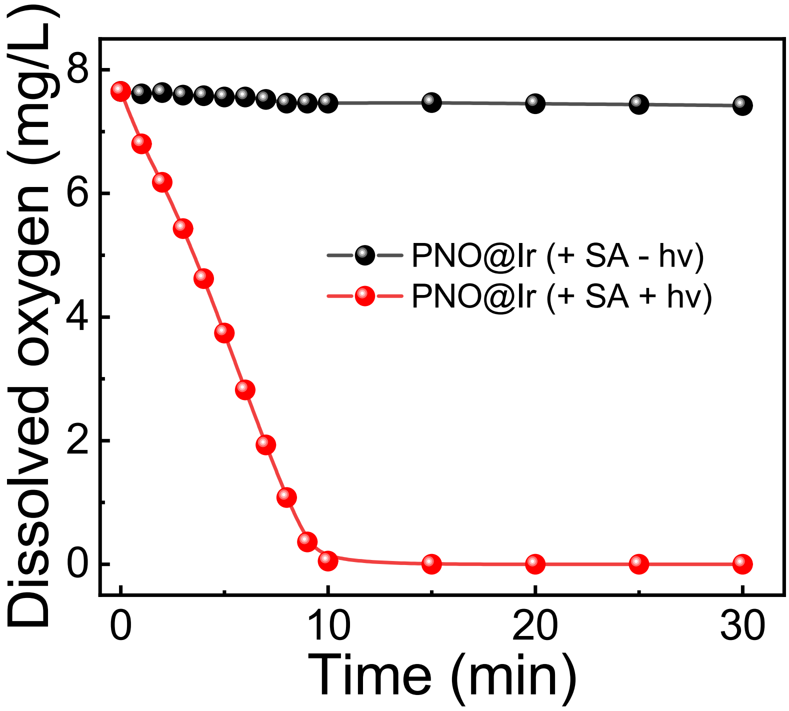

Fig. S14 Changes of oxygen concentrations of aqueous dispersions (0.2 g/L) PNO@Ir micelles in the presence of 10 mM sodium ascorbate with or without 500 nm light irradiation (30 mW/cm^2).

Note. The produced singlet oxygen under red light irradiation was consumed by sodium ascorbate, leading to a decreased dissolved oxygen in solutions.

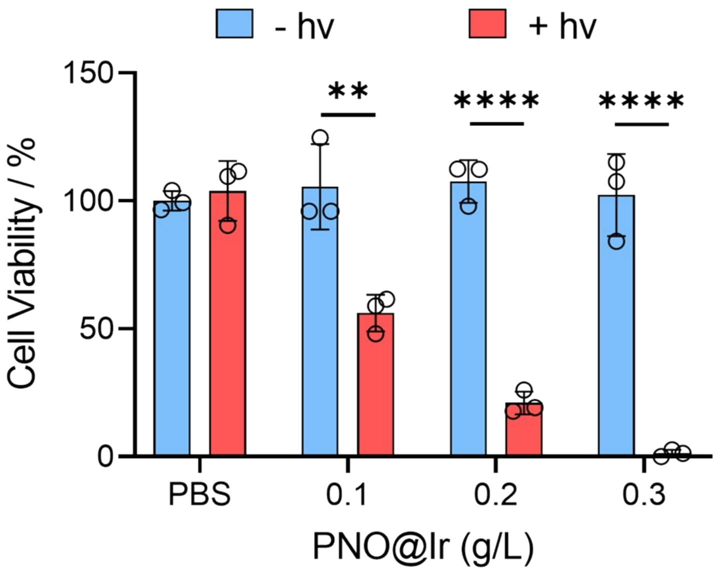

Fig. S15 MRSA viability after treatment with PNO@Ir micelles without or with 500 nm irradiation for 30 min. Data are shown as the mean ± s.d. (n = 3); ***p* < 0.01, ****p* < 0.001, *****p* < 0.0001.

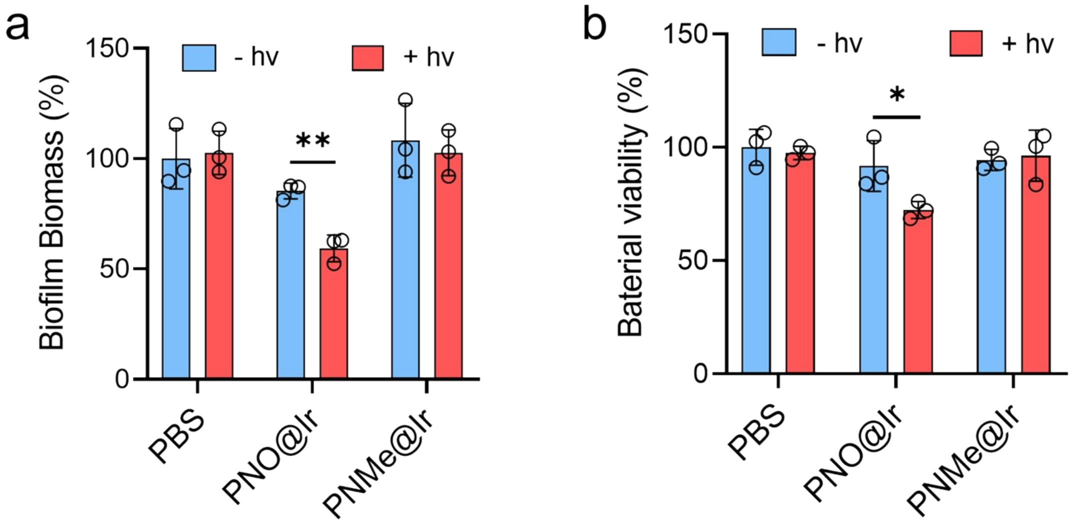

Fig. S16 (a) Bacterial biomass of *P. aeruginosa* PAO1 biofilms by crystal violet staining and (b) corresponding bacterial viability after treatment with PBS, PNO@Ir, and PNMe@Ir micelles without or with 500 nm light irradiation for 30 min under hypoxic conditions, respectively. Data are shown as the mean ± s.d. (n = 3); $^{*}p < 0.05$, $^{**}p < 0.01$.

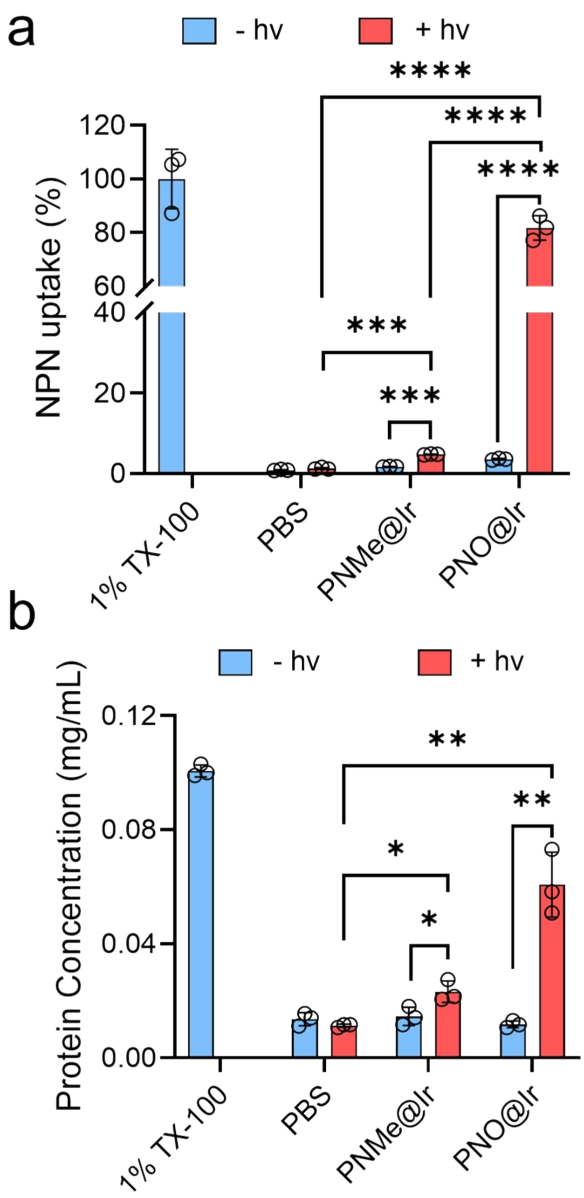

Fig. S17 (a) NPN uptake, (b) protein leakage assay of MRSA after treatment with PNO@Ir, PNMe@Ir micelles (0.2 g/L) without or with 500 nm irradiation for 30 min. In all cases, 1% TX-100 and PBS were used as the positive and negative controls, respectively. Data are shown as the mean ± s.d. ($n = 3$); *$p < 0.05$, **$p < 0.01$, ***$p < 0.001$, **$p < 0.0001$.

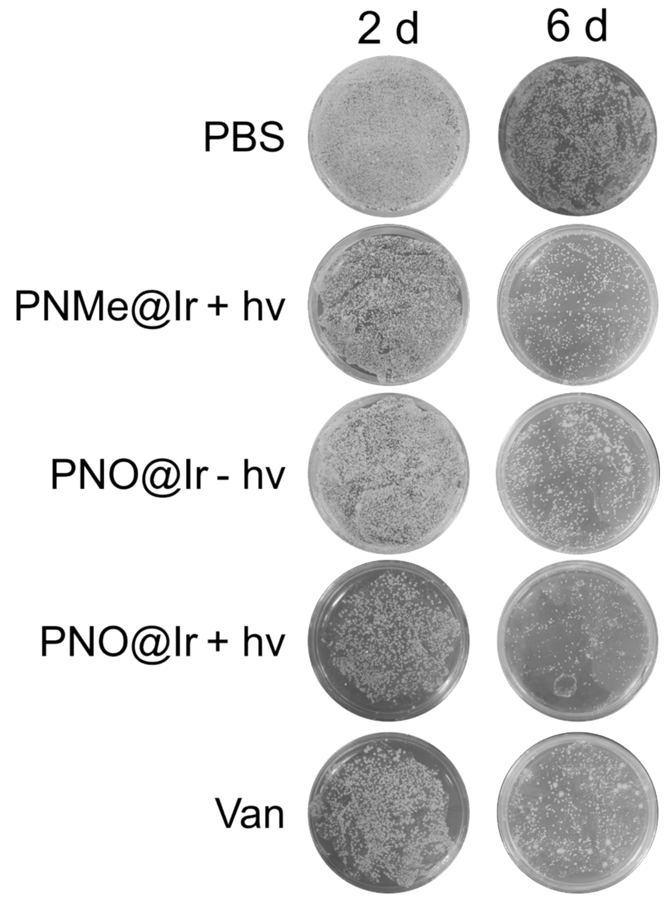

Fig. S18 Photographs of bacterial colonies on the agar plates of the wound tissues with varying treatments on day 2 and day 6.

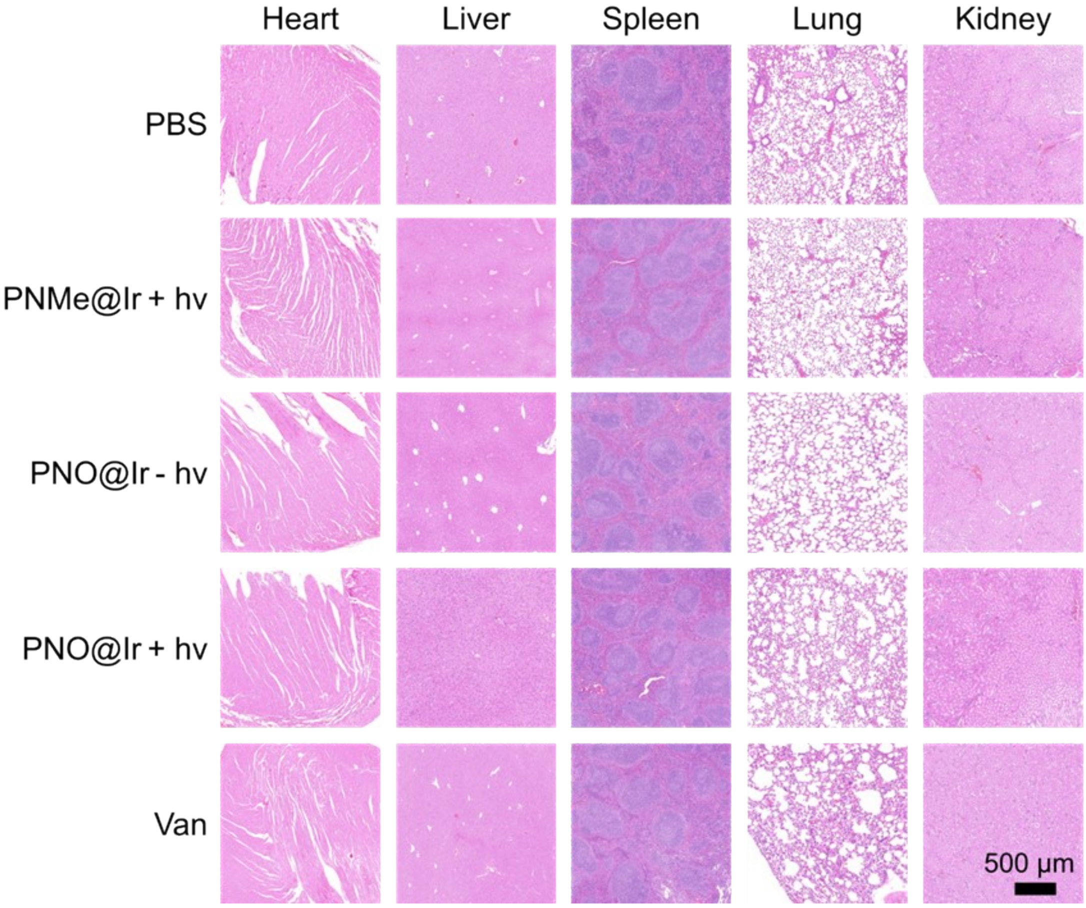

Fig. S19 Hematoxylin and eosin (H&E) staining of major organs (heart, liver, spleen, lung, and kidney) on day 6 of mice infected with MRSA receiving varying treatments. Scale bar: 500 µm.

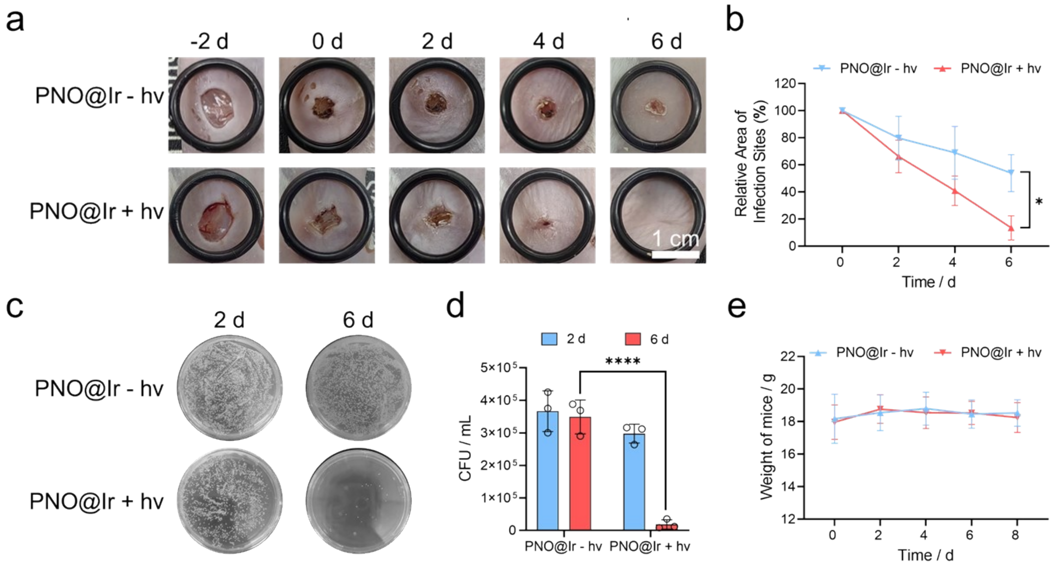

Fig. S20 (a) Representative images of the wound during the treatment process and (b) quantitative analysis of the infected areas receiving different treatments. Data are shown as the mean ± s.d. (n = 3); *$p < 0.05$ compared with the PNO@Ir (+ hv) group. (c) Photographs of bacterial colonies on the agar plates of the wound tissues with varying treatments on day 2 and day 6. (d) Bacterial colony-forming unit separated from wound tissues with varying treatments. Data are shown as the mean ± s.d. (n = 3); ****$p < 0.0001$, compared with the group receiving PNO@Ir (+ hv) treatment on day 6. (e) Changes of body weights of MRSA biofilm-infected mice after different treatments. In all cases, the micelle concentrations were 0.3 g/L, respectively.

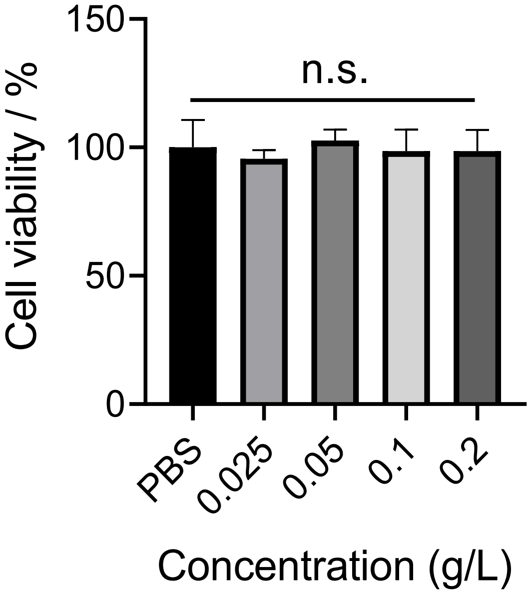

Fig. S21 Cell viability of human umbilical vein endothelial cells (HUVECs) as determined by MTT assay after 24 h incubation with PNO@Ir. n.s. not significant versus the PBS group.